Journal of Science: Advanced Materials and Devices 1 (2016) 527–530

Contents lists available at ScienceDirect

Journal of Science: Advanced Materials and Devices

journal homepage: www.elsevier.com/locate/jsamd

Original Article

Characterizing magnesium–silicon binaries in Al–Mg–Si supersaturated solid solution by first-principles calculations

Tran Doan Huan [a,*], Nam Ba Le [b]

[a] Department of Materials Science & Engineering and Institute of Materials Science, University of Connecticut, 97 North Eagleville Road, Unit 3136, Storrs, CT 06269-3136, USA
[b] Institute of Engineering Physics, Hanoi University of Science and Technology, 1 Dai Co Viet Road, Hanoi 100000, Viet Nam

ARTICLE INFO

Article history:
Received 19 August 2016
Received in revised form
13 September 2016
Accepted 15 September 2016
Available online 23 September 2016

Keywords:
Al–Mg–Si solid solution
Mg–Si binaries
Stability
Density functional theory

ABSTRACT

Magnesium silicide Mg_2Si is a well-studied binary of Mg and Si due to its potential technological applications like infrared photonic and thermoelectric. In many experimental scenarios, e.g., in supersaturated solid solution of Al–Mg–Si, some other Mg-Si binaries, e.g., Mg_9Si_5 and Mg_5Si_6, co-exist with Mg_2Si. It was then computationally found that Mg_9Si_5 and Mg_5Si_6 are thermodynamically favorable under some non-zero pressures. Other than this, very little is known about these two new binaries. This paper aims to unveil some structural, electronic, and vibrational properties of Mg_9Si_5 and Mg_5Si_6, providing some information that may be useful for further possible investigations on the Al–Mg–Si solid solution.

1. Introduction

At ambient conditions, magnesium silicide Mg_2Si, which crystalizes in the cubic $Fm\overline{3}m$ structure, is a narrow-gap semiconductor before transforming to a variety of metallic phases at elevated pressures [1–5]. This binary is promising for a variety of applications, including infrared photonic and thermoelectric [6–10] Two relatives of Mg_2Si, namely Mg_9Si_5 and Mg_5Si_6, were experimentally observed as the β' and β'' in the supersaturated solid solution of Al–Mg–Si [11–15]. Unlike Mg_2Si, which has extensively been studied [1–10,16,17], litle was known about Mg_9Si_5 and Mg_5Si_6. The former, e.g., Mg_9Si_5, adopts the hexagonal $P6_3/m$ symmetry and is higher in energy than the high-pressure hexagonal $P6_3/mmc$ structure of Mg_2Si, according to a computational study [12]. The structure of Mg_5Si_6 was also resolved experimentally [14,15] to belong to the $C2/m$ space group.

The phase diagram of Mg_2Si at $\simeq 10$ GPa and above is quite rich with a number of contradicting reports. In short, a variety of different structural phases have been reported for Mg_2Si at these elevated pressures [1–5,16–18]. Considering their convex hull, which is constructed from first-principles calculations, it was recently suggested [18] that between 6 GPa and 24 GPa, Mg_9Si_5 can transform to Mg_2Si, and vice versa, without energy cost. Furthermore, Mg_5Si_6 in their $C2/m$ is thermodynamically stable at 12 GPa and above [18]. Presumably, some sorts of internal pressure in the Al–Mg–Si supersaturated solid solution may stabilize Mg_9Si_5 and Mg_5Si_6. This may also be the reason behind the unclear picture of high-pressure structural phases of Mg_2Si.

This paper is designed to characterize Mg_9Si_5 and Mg_5Si_6 by first-principles computations. Given that the phase diagram of Mg_2Si at high pressures remains largely unclear [18], we aim to some comparisons between the X-ray diffraction (XRD) patterns, the electronic structures, and the vibration-related properties of these binaries with those of Mg_2Si. We anticipate that the information provided by this work may help to identify the actual binaries of Mg and Si that are experimentally realized.

2. Calculation details

Calculations reported in this work were performed within the density functional theory (DFT) formalism [19,20] as implemented in *Vienna Ab Initio Simulation Package* (VASP) [21,22]. As described elsewhere [18], we used the semilocal Perdew–Burke–Ernzerhof functional [23] for the exchange-correlation energies, a 9 × 9 × 9 Monkhorst-Pack mesh [24] for sampling the Brillouin zone, and an energy cutoff of 500 eV for the plane-wave basis set. For all the

* Corresponding author.
E-mail address: huan.tran@uconn.edu (T.D. Huan).
Peer review under responsibility of Vietnam National University, Hanoi.

http://dx.doi.org/10.1016/j.jsamd.2016.09.002

structures, the cell and the atomic degrees of freedoms were optimized until the residual forces become smaller than 10^{-2} eV/Å. This setting typically leads to a convergence of less than 1 meV/atom in the DFT total energy E_{DFT}.

To examine the dynamical stability of the structures, their phonon band structures were prepared with PHONOPY [25,26]. Within the suppercell approach implemented in this package, atomic forces are calculated for the equilibrium structures with certain displacements introduced. The dynamical matrix was then constructed and diagonalized, returning the phonon dispersion cirves in the k space. The XRD results were generated using FULLPROF suite [27] while some fugures were rendered using VESTA [28].

3. Results and discussions

3.1. Materials structures and thermodynamic stability

According to Ref. [18], Mg_5Si_6 is thermodynamically stable at 12 GPa and above while Mg_9Si_5 and Mg_2Si can co-exist between 6 GPa and 24 GPa. This assessment was based upon the enthalpy calculated by DFT at zero temperature ($T = 0$). We strive to characterize Mg_5Si_6 and Mg_9Si_5 at finite temperatures by computing the Gibbs free energy as [29]

$$G(P,T) = E_{\rm DFT} + F_{\rm vib}(T) + PV. \quad (1)$$

here, P is the pressure and V is the volume of the simulation cell. $F_{\rm vib}(T)$ is the vibrational free energy, which can be computed from the phonon density of states $g(\omega)$ as [29].

$$F_{\rm vib}(T) = 3Nk_BT\int_0^\infty d\omega g(\omega)\ln\left[2\sinh\left(\frac{\hbar\omega}{2k_BT}\right)\right]. \quad (2)$$

In this expression, $3N$ is the number of degrees of freedom, k_B the Boltzmann, and $\hbar$ the reduced Planck constant. The phonon density of states $g(\omega)$ can be calculated when the phonon band structure is determined in Section 3.3. We consider the thermodynamic stability of the compounds at 0 GPa and 15 GPa. At 0 GPa, Mg_2Si is in the cubic $Fm\bar{3}m$ phase while at 15 GPa, it is in the orthorhombic $Pnma$ phase [18]. The lattice parameters of Mg_5Si_6 and Mg_9Si_5 obtained by DFT calculations at both 0 and 15 GPa are also reported in Table 1.

We first show in Fig. 1 the convex hull constructed from the Gibbs free energy calculated, taking the $P6_3/mmc$ phase of Mg and the $Fd\bar{3}m$ phase of Si as the reference. Results at 0 K are consistent with those reported in Ref. [18]. At elevated temperatures (300 K and 500 K), Mg_2Si always lies on the straight line between Mg_9Si_5 and Si, indicating that even at finites temperatures, Mg_9Si_5 and Mg_2Si can transform from one to the other without energy cost.

Fig. 2 shows the simulated XRD patterns of Mg_2Si, Mg_9Si_5, and Mg_5Si_6 at 15 GPa, revealing a significant similarity within the region between 35° and 50°. Mg_2Si and Mg_9Si_5 have two major reflections at 37° and 39° while Mg_9Si_5 and Mg_5Si_6 share a reflection at 48°. However, there are also noticeable differences in other regions of the XRD patterns. Therefore, although Mg_2Si and Mg_9Si_5 are essentially similar in terms of free energy, they may still be identified based upon carefully examining the measured XRD data.

Table 1
Structural parameters calculated for Mg_9Si_5 ($P6_3/m$ phase) and Mg_5Si_6 ($C2/m$ phase) at 0 and 15 GPa.

Material	P (GPa)	a (Å)	b (Å)	c (Å)	β (°)
Mg_9Si_5	0	7.08	7.08	12.11	90
Mg_9Si_5	15	6.71	6.71	11.44	90
Mg_5Si_6	0	14.91	4.08	6.80	110.2
Mg_5Si_6	15	14.26	3.87	6.39	109.1

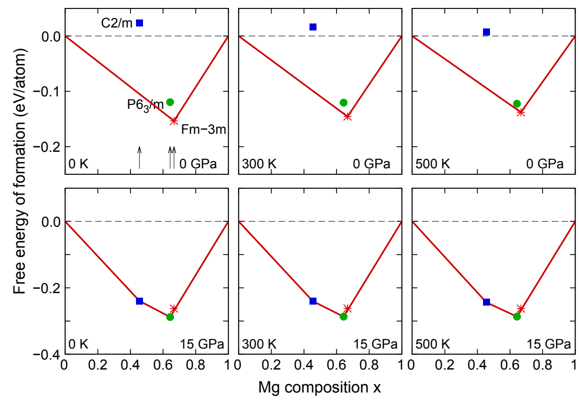

Fig. 1. Convex hull constructed from the Gibbs free energy computed for Mg_2Si, Mg_9Si_5, and Mg_5Si_6 at 0 GPa (top row) and 15 GPa (bottom row). Three arrows placed at $x = 0.455$, 0.643, and 0.667 indicate the Mg composition of Mg_5Si_6, Mg_9Si_5, and Mg_2Si, respectively.

3.2. Electronic structures

At zero pressure, Mg_2Si is in its cubic $Fm\bar{3}m$ semiconducting phase with a band gap of ≃0.7 eV [30]. Starting from about 6 GPa, Mg_2Si becomes metallic. It is therefore interesting to examine if Mg_9Si_5 and Mg_5Si_6 are semiconducting or metallic at the pressures that are expected to exist [18]. For this reason, we show in Fig. 3 the calculated the electronic densities of states of the $Pnma$ phase of Mg_2Si, the $P6_3/m$ phase of Mg_9Si_5, and the $C2/m$ phase of Mg_5Si_6 at 15 GPa. Clearly, all of these binaries are metallic at this pressure. We anticipate that for the whole range of pressure in which Mg_9Si_5 and Mg_5Si_6 may exist, they are also metallic. Further examination on their transport properties may also be carried out by computations as performed for Mg_2Si in Ref. [18].

3.3. Vibrational properties

The lattice vibration of a crystal structure encodes some useful information that is related to material properties. By examining the phonon dispersions, one may access the dynamically stability of a

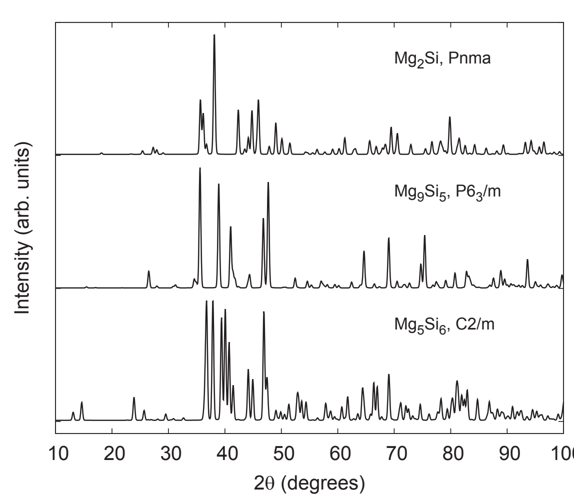

Fig. 2. XRD patterns of Mg_2Si ($Pnma$ phase), Mg_9Si_5 ($P6_3/m$ phase), and Mg_5Si_6 ($C2/m$ phase) at 15 GPa. Simulations were performed at the Cu Kα wavelength (1.54 Å).

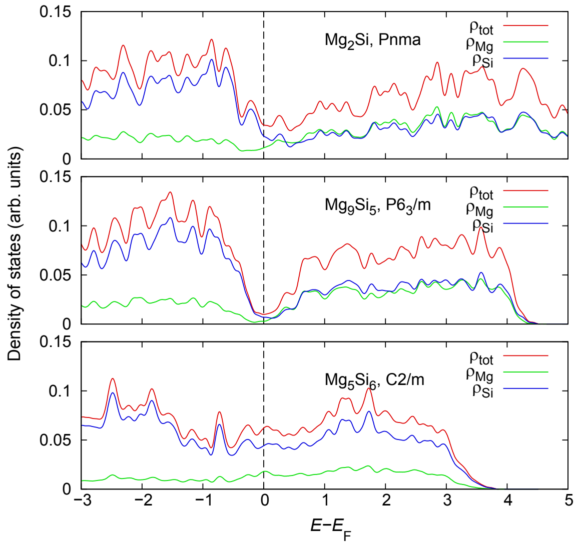

Fig. 3. Electronic density of states (DOS) of Mg_9Si_5, Mg_5Si_6, and Mg_2Si calculated at 15 GPa. The total DOS ρ_{tot} is also decomposed into ρ_{Mg} and ρ_{Si}, the projected DOS on the Mg and Si sites. Dashed lines indicate the Fermi level.

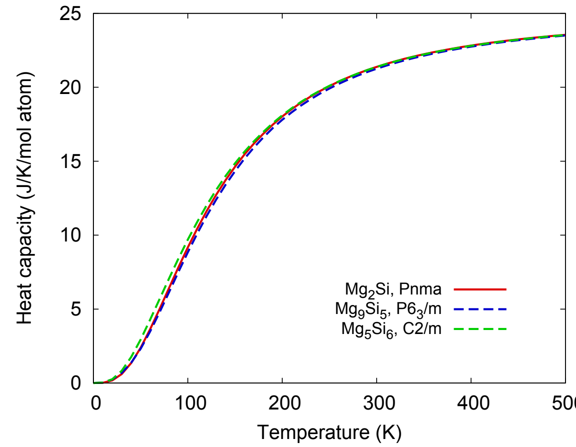

Fig. 5. Constant volume heat capacity calculated for C_v of Mg_9Si_5, Mg_5Si_6, and Mg_2Si at 15 GPa.

structural model. This step is now becoming increasingly relevant as a number of structure models proposed theoretically and/or experimentally are dynamically unstable [31]. While phonon dispersion cuves may be measured by inelastic neutron scattering, *state-of-the-art* computational techniques, especially those based from DFT calculations, are now capable to obtain such information within the harmonic approximation. Although phonon calculations are typically expensive, they are a quite common practice, given that other important physical quantities, e.g., free energies and heat capacity, can also be estimated from the obtained results [18,29,31,32].

We show in Fig. 4 the phonon band structures calculated for Mg_9Si_5 ($P6_3/m$ phase) and Mg_5Si_6 ($C2/m$ phase) at 0 and 15 GPa. Because no imaginary phonon mode could be found in the Brillouin zones, one can conclude that both the $P6_3/m$ phase of Mg_9Si_5 and the $C2/m$ phase of Mg_5Si_6 are dynamically stable at the pressures examined. In other words, these structure models correspond to the minima of the potential energy surface, and therefore could be experimentally relevant. In addition, the expansion of the whole dispersion structure from 0 GPa to 15 GPa is a natural consequence of the structure compression under pressure.

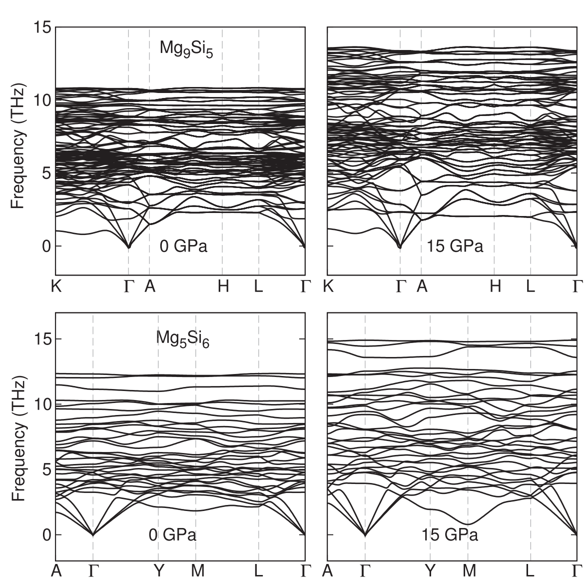

Fig. 4. Phonon band structures of Mg_9Si_5 ($P6_3/m$ phase, top row) and Mg_5Si_6 ($C2/m$ phase, bottom row) at 0 and 15 GPa.

From the obtained phonon dispersion curves, the constant volume heat capacity C_v can also be computed as

$$C_v(T) = 3Nk_B \int_0^\infty d\omega g(\omega) \left(\frac{\hbar\omega}{k_B T}\right)^2 \frac{\exp(\hbar\omega/k_B T)}{[\exp(\hbar\omega/k_B T) - 1]^2}. \quad (3)$$

In Fig. 5, C_v calculated for Mg_9Si_5, Mg_5Si_6, and Mg_2Si at 15 GPa is shown. It turns out that for high temperature, the heat capacities of Mg_9Si_5, Mg_5Si_6, and Mg_2Si are essentially similar. At about 100 K and below, the specific heat C_v of Mg_5Si_6 is higher than that of Mg_9Si_5 and Mg_2Si by roughly 2%, a detectable quantities from the experimental point of view.

4. Summary

We present a computational study on Mg_9Si_5 and Mg_5Si_6, the binaries reported to co-exist with Mg_2Si in some experiments. At 0 GPa and 15 GPa, these binaries are found to be thermodynamically and dynamically stable. Especially, we confirm that within a wide range of finite pressure and temperature, Mg_2Si and Mg_9Si_5 are essentially equivalent in terms of free energy. Electronic structure calculations reveal that similar to Mg_2Si, both Mg_9Si_5 and Mg_5Si_6 are metallic at 15 GPa. Although the XRD patterns of Mg_9Si_5 and Mg_2Si share some noticeable reflections, we anticipate that the computational descriptions may supply useful information for the identification of these binaries in further experiments.

References

[1] E.Y. Tonkov, High Pressure Phase Transformations: A Handbook, Gordan and Breach Science, Philadelphia, US, 1992.
[2] J.-H. Hao, Z.-G. Guo, Q.-H. Jin, First principles calculation of structural phase transformation in Mg_2 Si at high pressure, Solid State Commun. 150 (2010) 2299–2302.
[3] F. Yu, J.-X. Sun, W. Yang, R.-G. Tian, G.-F. Ji, A study of the phase transitions, electronic structures and optical properties of Mg_2 Si under high pressure, Solid State Commun. 150 (2010) 620–624.
[4] F. Zhu, X. Wu, S. Qin, J. Liu, A re-investigation on pressure-induced phase transition of Mg_2 Si, Solid State Commun. 152 (2012) 2160–2164.
[5] W. Ren, Y. Han, C. Liu, N. Su, Y. Li, B. Ma, Y. Ma, C. Gao, Pressure-induced semiconductor-metal phase transition in Mg_2 Si, Solid State Commun. 152 (2012) 440–442.

[6] H. Udono, H. Tajima, M. Uchikoshi, M. Itakura, Crystal growth and characterization of Mg_2 Si for IR-detectors and thermoelectric applications, Jpn. J. Appl. Phys. 54 (2015), 07JB06.
[7] H. Udono, Y. Yamanaka, M. Uchikoshi, M. Itakura, Infrared photoresponse from pn-junction Mg_2 Si diodes fabricated by thermal diffusion, J. Phys. Chem. Solids 74 (2013) 311.
[8] V.K. Zaitsev, M.I. Fedorov, E.A. Gurieva, I.S. Eremin, P.P. Konstantinov, A.Y. Samunin, M.V. Vedernikov, Highly effective Mg_2 $2Si_{1-x}$ Snx thermoelectrics, Phys. Rev. B 74 (2006) 045207.
[9] W. Liu, X. Tan, K. Yin, H. Liu, X. Tang, J. Shi, Q. Zhang, C. Uher, Convergence of conduction bands as a means of enhancing thermoelectric performance of n-type Mg_2 $2Si_{1-x}$ Sn_x solid solutions, Phys. Rev. Lett. 108 (2012) 166601.
[10] N.V. Morozova, S.V. Ovsyannikov, I.V. Korobeinikov, A.E. Karkin, K. Takarabe, Y. Mori, S. Nakamura, V.V. Shchennikov, Significant enhancement of thermoelectric properties and metallization of al-doped Mg_2 Si under pressure, J. Appl. Phys. 115 (2014) 213705.
[11] M.A. van Huis, J.H. Chen, H.W. Zandbergen, M.H.F. Sluiter, Phase stability and structural relations of nanometer-sized, matrix-embedded precipitate phases in Al-Mg-Si alloys in the late stages of evolution, Acta Mater 54 (11) (2006) 2945–2955.
[12] R. Vissers, M.A. van Huis, J. Jansen, H.W. Zandbergen, C.D. Marioara, S.J. Andersen, The crystal structure of the β' phase in Al-Mg-Si alloys, Acta Mater 55 (11) (2007) 3815–3823.
[13] S. Ji, M. Tanaka, S. Zhang, S. Yamanaka, High pressure synthesis and superconductivity of the ternary compounds $Mg(Mg_{1-x}$ $Al_x)Si$ with the anti-cotunnite structure, Inorg. Chem. 51 (19) (2012) 10300–10305.
[14] H.W. Zandbergen, S.J. Andersen, J. Jansen, Structure determination of Mg_5 Si_6 particles in Al by dynamic electron diffraction studies, Science 277 (1997) 1221.
[15] S.J. Andersen, H.W. Zandbergen, J. Jansen, C. Traeholt, U. Tundal, O. Reiso, The crystal structure of the β'' phase in al-mg-si alloys, Acta Mater 46 (9) (1998) 3283–3298, http://dx.doi.org/10.1016/S1359-6454(97)00493-X.
[16] P. Cannon, E.T. Conlin, Magnesium compounds: new dense phases, Science 145 (1964) 487–489.
[17] T. Peun, J. Lauterjung, E. Hinze, High pressure and high temperature investigations on intermetallic compounds using energy-dispersive x-ray powder diffraction, Nucl. Instr. Methods Phys. Res. B 97 (1–4) (1995) 483–486.
[18] T.D. Huan, V.N. Tuoc, N.B. Le, V.N. Minh, L.M. Woods, High-pressure phases of Mg_2 Si from first principles, Phys. Rev. B 93 (2016) 094109.
[19] P. Hohenberg, W. Kohn, Inhomogeneous electron gas, Phys. Rev. 136 (1964). B864.
[20] W. Kohn, L. Sham, Self-consistent equations including exchange and correlation effects, Phys. Rev. 140 (1965). A1133.
[21] G. Kresse, J. Hafner, Ab initio molecular dynamics for liquid metals, Phys. Rev. B 47 (1993) 558.
[22] G. Kresse, Ab initio molekular dynamik für flüssige metalle (Ph.D. thesis), Technische Universität Wien, 1993.
[23] J.P. Perdew, K. Burke, M. Ernzerhof, Generalized gradient approximation made simple, Phys. Rev. Lett. 77 (1996) 3865.
[24] H.J. Monkhorst, J.D. Pack, Special points for brillouin-zone integrations, Phys. Rev. B 13 (1976) 5188.
[25] A. Togo, F. Oba, I. Tanaka, First-principles calculations of the ferroelastic transition between rutile-type and cacl2-type sio2 at high pressures, Phys. Rev. B 78 (2008) 134106.
[26] K. Parlinski, Z.Q. Li, Y. Kawazoe, First-principles determination of the soft mode in cubic zro2, Phys. Rev. Lett. 78 (1997) 4063.
[27] J. Rodríguez-Carvajal, Recent advances in magnetic structure determination by neutron powder diffraction, Physica B 192 (1993) 55.
[28] K. Momma, F. Izumi, VESTA: a three-dimensional visualization system for electronic and structural analysis, J. Appl. Crystallogr. 41 (2008) 653.
[29] T.D. Huan, Evaluation of Crystal Free Energy with Lattice Dynamics, arXiv Preprint, 2015 arXiv:1506.09189.
[30] D.M. Rowe, CRC Handbook of Thermoelectrics, CRC Press, USA, 1995.
[31] H.D. Tran, M. Amsler, S. Botti, M.A.L. Marques, S. Goedecker, First-principles predicted low-energy structures of $NaSc(BH_4)_4$, J. Chem. Phys. 140 (2014) 124708.
[32] T.D. Huan, M. Amsler, R. Sabatini, V.N. Tuoc, N.B. Le, L.M. Woods, N. Marzari, S. Goedecker, Thermodynamic stability of alkali metal/zinc double-cation borohydrides at low temperatures, Phys. Rev. B 88 (2013) 024108.